Chaperone-mediated reflux of secretory proteins to the cytosol during endoplasmic reticulum stress

Aeid Igbaria[a,b,c,1], Philip I. Merksamer[a,b,c,d,1], Ala Trusina[e], Firehiwot Tilahun[a,b,c], Jeffrey R. Johnson[d,f], Onn Brandman[c,f,g], Nevan J. Krogan[d,f], Jonathan S. Weissman[c,f,g], and Feroz R. Papa[a,b,c,2]

[a]Department of Medicine, University of California, San Francisco, CA 94143; [b]Diabetes Center, University of California, San Francisco, CA 94143; [c]Quantitative Biosciences Institute, University of California, San Francisco, CA 94143; [d]Gladstone Institute of Virology and Immunology, San Francisco, CA 94158; [e]Center for Models of Life, Niels Bohr Institute, University of Copenhagen, DK 2100 Copenhagen, Denmark; [f]Department of Cellular and Molecular Pharmacology, University of California, San Francisco, CA 94143; and [g]Howard Hughes Medical Institute, University of California, San Francisco, CA 94143

Edited by Randy Schekman, University of California, Berkeley, CA, and approved April 5, 2019 (received for review March 18, 2019)

Diverse perturbations to endoplasmic reticulum (ER) functions compromise the proper folding and structural maturation of secretory proteins. To study secretory pathway physiology during such "ER stress," we employed an ER-targeted, redox-responsive, green fluorescent protein—eroGFP—that reports on ambient changes in oxidizing potential. Here we find that diverse ER stress regimes cause properly folded, ER-resident eroGFP (and other ER luminal proteins) to "reflux" back to the reducing environment of the cytosol as intact, folded proteins. By utilizing eroGFP in a comprehensive genetic screen in *Saccharomyces cerevisiae*, we show that ER protein reflux during ER stress requires specific chaperones and cochaperones residing in both the ER and the cytosol. Chaperone-mediated ER protein reflux does not require E3 ligase activity, and proceeds even more vigorously when these ER-associated degradation (ERAD) factors are crippled, suggesting that reflux may work in parallel with ERAD. In summary, chaperone-mediated ER protein reflux may be a conserved protein quality control process that evolved to maintain secretory pathway homeostasis during ER protein-folding stress.

reflux | UPR | ERAD | endoplasmic reticulum stress

In eukaryotic cells, secretory and membrane proteins begin translation in the cytoplasm and are then either co- or post-translationally translocated through the Sec61 translocon channel into the endoplasmic reticulum (ER) (1). The ER is crowded with molecular chaperones and protein-modifying enzymes that promote folding and structural maturation of these nascent, maturing secretory pathway client proteins as they traverse the early secretory pathway (2). To ensure stringent quality control over these secretory cargoes, those proteins that fail to correctly fold and mature are retrieved from the ER, ubiquitylated, and degraded by the 26S proteasome in the cytosol in a process termed ER-associated degradation (ERAD) (3).

Diverse environmental perturbations or genetic mutations can elevate misfolding of maturing proteins in the ER. During such "ER stress," cells trigger an intracellular signaling pathway called the unfolded protein response (UPR) that augments protein-folding reactions through transcriptional up-regulation of genes encoding ER chaperones, oxidoreductases, lipid biosynthetic enzymes, and ERAD components (4). If these adaptive UPR outputs prove successful in reducing the concentration of unfolded proteins in the ER, cells become restored to a homeostatic state (5).

However, because the UPR's activating inputs—(i.e., unfolded proteins)—are unfeasible to monitor in vivo, it is often unclear if and when the UPR has successfully restored homeostasis. To address this problem orthogonally, we previously developed an ER-targeted redox-sensitive green fluorescent protein (GFP)—called eroGFP—to follow oxidative protein folding in the ER, reasoning that this essential ER physiological function may deviate during ER stress and thereby provide an independent measure of ER health (i.e., that is distinct from solely measuring UPR activation). We previously showed that differential, real-time, quantitative eroGFP changes occurred dynamically upon general loss of ER protein-folding homeostasis in wild-type cells and in a small, select group of yeast mutants (6). Here, using high-throughput flow cytometry, we have extended this analysis to the entire yeast genome to query nearly all non-essential and essential genes. Through this screen, we have identified and characterized a process by which eroGFP, and a number of ER-resident luminal proteins, are "refluxed" back to the cytosol as intact folded proteins during ER stress. The protein reflux process occurs independent of Hrd1 and Doa10 E3 ligases and does not require polyubiquitinylation. Instead, ER protein reflux requires specific chaperones and cochaperones both in the ER and cytosol, and is reminiscent of a molecular ratchet that promotes translocation, but proceeding vectorially in the opposite direction (7, 8).

Results

ER-to-Cytosol Reflux of ER-Targeted eroGFP. Designed to be a reporter of ambient redox potential, eroGFP has an engineered reversible disulfide bond that alters fluorescence excitability from its two maxima of 490 and 400 nm, such that reduction of the disulfide increases fluorescence from 490 nm excitation, at the expense of that from 400 nm (6, 9). Thus, eroGFP is ratiometric by excitation,

Significance

Approximately one-third of eukaryotic proteins are synthesized on ribosomes attached to the endoplasmic reticulum (ER) membrane. Many of these polypeptides co- or posttranslationally translocate into the ER, wherein they fold and mature. An ER quality control system proofreads these proteins by facilitating their folding and modification, while eliminating misfolded proteins through ER-associated degradation (ERAD). Yet the fate of many secretory proteins during ER stress is not completely understood. Here, we uncovered an ER stress-induced "protein reflux" system that delivers intact, folded ER luminal proteins back to the cytosol without degrading them. We found that ER protein reflux works in parallel with ERAD and requires distinct ER-resident and cytosolic chaperones and cochaperones.

Author contributions: A.I., P.I.M., and F.R.P. designed research; A.I., P.I.M., F.T., J.R.J., and O.B. performed research; A.T., O.B., N.J.K., and J.S.W. contributed new reagents/analytic tools; A.I., P.I.M., A.T., J.R.J., and F.R.P. analyzed data; and A.I., P.I.M., and F.R.P. wrote the paper.

The authors declare no conflict of interest.

This article is a PNAS Direct Submission.

[1]A.I. and P.I.M. contributed equally to this work.

[2]To whom correspondence should be addressed. Email: frpapa@medicine.ucsf.edu.

This article contains supporting information online at www.pnas.org/lookup/suppl/doi:10.1073/pnas.1904516116/-/DCSupplemental.

which facilitates internally controlled measurement of its oxidation state. Through flow cytometry, the eroGFP ratio—defined as fluorescence from excitation at 488 versus 405 nm in $\log_2$ space—can be measured in single yeast cells growing in populations (Fig. 1*A*). Targeted to the oxidizing environment of the ER through an N-terminal Kar2 signal peptide sequence (and retained in the organelle through a C-terminal HDEL sequence), eroGFP (which has a redox midpoint potential of −282 mV) is nearly completely oxidized at baseline. Treatment with hydrogen peroxide (H_2O_2) only slightly further decreases the eroGFP ratio (6). However, a wide dynamic range exists for reduction, since titration with increasing amounts of the reductant DTT—an ER stress agent—dose dependently increases the eroGFP ratio until the reporter becomes fully reduced (Fig. 1*B*). As previously shown, acute treatment of cells with (saturating) DTT causes rapid elevation of the eroGFP ratio to its new steady-state level due to in situ and complete reduction of the reporter (6) (*SI Appendix*, Fig. S1 *A*–*C*). Tunicamycin (Tm), which impairs N-linked protein glycosylation in the ER, also led to partial reduction of the eroGFP reporter, but with slower dynamics compared with treatment with DTT [as previously shown (6)] (*SI Appendix*, Fig. S1 *A*–*C*). Indeed, the general utility of the eroGFP tool is that it deflects differentially (by reduction) in response to diverse ER stress agents (including forced expression of unfolded secretory proteins) (6).

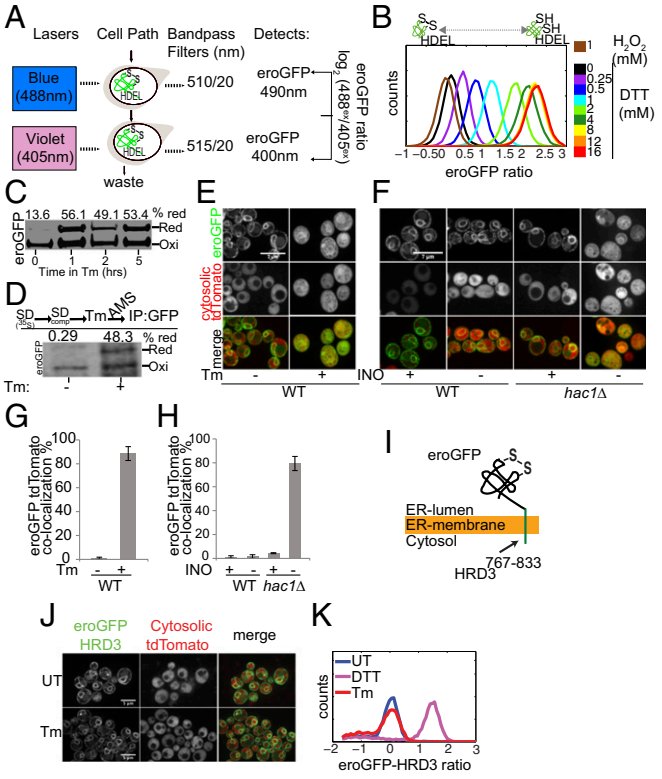

Fig. 1. ER-targeted eroGFP localizes to the cytosol during ER stress. (*A*) Schematic showing configuration of flow cytometer laser lines and filters used to measure eroGFP fluorescence excitation and emission. (*B*) eroGFP ratios for populations of wild-type cells treated with the indicated concentration of DTT or H_2O_2 for 20 min. (*C*) eroGFP redox state in WT cells treated with (6 μg/mL) Tm for the indicated time points. (*D*) eroGFP redox state after ^{35}S pulse–chase in WT cells treated with Tm for 2 h. Extracts were treated with AMS, immunoprecipitated with anti-GFP (IP:GFP), and resolved on nonreducing SDS/PAGE. (*E*) Confocal images of wild-type cells expressing eroGFP and cytosolic tdTomato treated with Tm for 2 h. (*F*) Confocal images of wild-type and *hac1*Δ yeast expressing eroGFP and cytosolic tdTomato starved for inositol (INO) for 8 h. (*G* and *H*) Quantification of Tm confocal images (*G*) and inositol confocal images (*H*). Error bars represent SEM of two independent experiments. (*I*) Schematic of HRD3-eroGFP. eroGFP was translationally fused to residues 767 to 833 of HRD3 to imbed eroGFP in the ER membrane. (*J*) Confocal images of WT cells expressing HRD3-eroGFP and cytosolic tdTomato treated with Tm for 2 h. UT, untreated. (*K*) Histograms of HRD3-eroGFP ratios for wild-type cells treated with 2 mM DTT for 20 min and Tm for 5 h.

Since our original study, which was based on single-cell interrogations using real-time flow cytometry, it was also reported that partial cytoplasmic localization of eroGFP occurs during expression of a mutant of the UPR master regulator, Ire1, that cannot deactivate the UPR (10); this result implied that cytoplasmic localization of the eroGFP reporter may occur due to a translocation defect under unresolved ER stress signaling. But in our original study, through using a yeast strain expressing a GAL1/10 promoter-driven eroGFP construct gene that no longer expresses new eroGFP after glucose shutoff, we had established that eroGFP reduction due to Tm provision occurred after the glucose shutoff (figure S7 in ref. 6). Thus, we had reasonably concluded that ER stress induced by Tm caused reduction of preexisting eroGFP that was already residing in the ER lumen.

We revisited these experimental systems by showing again that provision of Tm to wild-type yeast cells dynamically caused eroGFP reporter reduction (to ∼50% of basal levels) (detectable in a time course of 4-acetamido-4′-maleimidylstilbene-2,2′-disulphonic acid (AMS) modification, resolution on nonreducing SDS/PAGE, and then followed by immunoblotting against GFP) (Fig. 1*C*). Also, in a pulse–chase regime to label preexisting reporter, reduction was detectable within 2 h after Tm provision (i.e., when eroGFP reduction reaches its new steady state) (Fig. 1*D*). Next, to specifically track the cytoplasmic compartment with high sensitivity, we integrated a cytosolically disposed tdTomato reporter into eroGFP-expressing yeast and followed both reporters by fluorescence microscopy. Using this double-reporter system and a high-dose regime of Tm (6 μg/mL) provided for 2 h, we visually scored any cell showing merged eroGFP/cytosolic tdTomato as being "colocalized" (yellow overlay). This regime revealed significant numbers of cells with some eroGFP signal localized to the cytosol (Fig. 1 *E* and *G* and *SI Appendix*, Fig. S1*D*). However, we still observed significant eroGFP signal retained within the ER in these colocalized cells, which is consistent with the incomplete reduction of eroGFP that we had observed after Tm treatment by flow cytometry.

Because Tm is a severe nonphysiological stress, we next asked whether eroGFP localizes to the cytosol under a more physiological stress. To this end, we starved UPR-deficient yeast mutants (which are inositol auxotrophs) for inositol, which we previously found to cause reduction of eroGFP in subpopulations when measured by flow cytometry (6, 10). Relative to the Tm regime, we observed a smaller fraction of cells with eroGFP localized to the cytosol in inositol-starved *hac1*Δ mutants but not in control wild-type cells, which are prototrophs for inositol and retain eroGFP in the ER upon inositol starvation (Fig. 1 *F* and *H*).

To further test whether Tm-induced reduction of eroGFP occurred due to its exposure to the reducing cytosol, we constructed a variant of eroGFP that was fused to the transmembrane domain of the single-pass ER membrane protein Hrd3 such that the GFP domain remained topologically disposed inside the ER (Fig. 1*I*). This Hrd3-eroGFP reporter's fluorescence signal did not overlap with cytosolic tdTomato following Tm (Fig. 1*J*) and its oxidation state remained unperturbed under this treatment, while it could still be reduced in situ with DTT (Fig. 1*K*). Thus, altered (cytosolic) localization during ER stress is confined to a soluble form of eroGFP, and the oxidation change of this reporter occurs upon exposure to the reducing environment of the cytosol.

Two mechanisms could account a priori for localization of ER-targeted eroGFP in the cytosol during ER stress: (*i*) eroGFP that was en route to the ER may have become averted due to

disabled translocation into the organelle during ER stress, as was shown for other client proteins in a "preemptive" quality control pathway (11); or (*ii*) eroGFP already in the ER lumen may have been returned back to the cytosol during stress. To distinguish between these two possibilities, we engineered an N-linked glycosylation site into eroGFP in a 9-amino acid linker region between the GFP-coding sequence and the C-terminal HDEL retrieval sequence to follow the fate of the reporter after its glycosylation in the ER. We termed this variant eroGFP-Glyc (*SI Appendix*, Fig. S2*A*). As expected, in unstressed cells, eroGFP-Glyc migrates slower on SDS/PAGE compared with eroGFP, consistent with its glycosylation. Confirming this, treatment with the deglycosylase EndoH increased eroGFP-Glyc mobility such that it now comigrated with eroGFP (*SI Appendix*, Fig. S2*B*).

To then directly follow this reporter's fate after it was already resident in the ER lumen, we placed eroGFP-Glyc under control of the GAL1/10 promoter to rapidly cease de novo production with glucose. Quantitative PCR and pulse-label analysis confirmed that glucose provision halted transcription within the first 30 min and new protein synthesis by 2 h (*SI Appendix*, Fig. S2*C*). We estimated the half-life of eroGFP-Glyc based on a [^{35}S]methionine pulse-label experiment (*SI Appendix*, Fig. S2 *D* and *E*), and used this information to determine that the fraction of newly synthesized eroGFP is ∼6% of total eroGFP at 2 h from the shift to glucose (*SI Appendix*, Fig. S2*F*); thus, the majority of the reporter should be preexisting. As with eroGFP, we again confirmed that this preexisting eroGFP-Glyc (i.e., post glucose addition) became localized to the cytosol during the Tm treatment of 2 h (*SI Appendix*, Fig. S2*G*). Moreover, we reasoned that if this pool of preexisting eroGFP-Glyc had already entered and then later exited the ER, the beta-aspartylglycosylamine bond at its N-glycan tree should become cleaved in the cytosol by deglycosylating enzyme peptide N-glycanase—PNGase—thus converting the asparagine at the glycosylation site to an aspartate residue (12). To test this, we used 2D gel electrophoresis to monitor isoelectric shifts that would indicate an asparagine-to-aspartate conversion. After treatment with Tm, we observed that the faster-migrating deglycosylated species have a lower isoelectric point (i.e., more acidic, as expected) than the slower-migrating glycosylated species, suggesting an asparagine-to-aspartate conversion (*SI Appendix*, Fig. S2*H*). Confirming this, the shift with Tm is superimposable when eroGFP-Glyc is treated enzymatically with PNGase, which cleaves the beta-aspartylglycosylamine bond, and also with an eroGFP-Glyc variant in which an aspartate has replaced the asparagine (eroGFPND) at the glycosylation site. In addition, we used mass spectrometry to measure deamidation of the deglycosylated asparagine. While a cytosolic version of the reporter lacking the signal peptide but bearing the C-terminal glycosylation signal, termed cytoGFP-Glyc, displayed low levels of deamidation under Tm, eroGFP-Glyc showed a 200-fold relative increase in deamidation of the Asn residue in the relevant peptide (*SI Appendix*, Fig. S2*I*). For comparison, eroGFP-Glyc treated with PNGase, which should yield the theoretical maximum level of deamidation, displayed a 1,000-fold relative increase.

Together, the aforementioned data implied that a significant fraction of eroGFP (and eroGFP-Glyc) was already resident and properly folded in the ER, whereupon the reporter was subsequently removed back to the reducing environment of the cytosol during ER stress. To confirm this finding visually (i.e., directly), we constructed an ER-targeted photoactivatable fluorescent protein (ER-mEos3.2)-expressing yeast strain to specifically follow the fate of an ER-resident reporter while ignoring contributions from new protein synthesis and translocation (Fig. 2*A*). mEos3.2 is a monomeric photoactivatable fluorescent protein that has an excitation maximum at 507 nm (green) (13). A UV pulse will optically highlight the existing pool of folded reporter by shifting the excitation maximum to 573 nm (red)

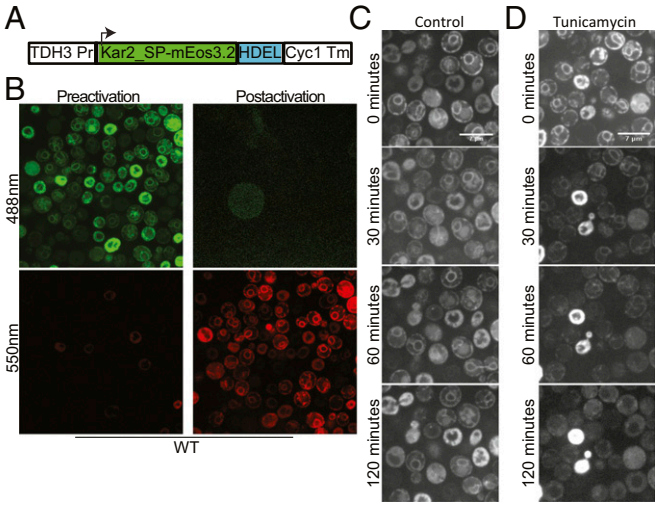

Fig. 2. Preexisting yemEos3 reporter is refluxed from the ER to the cytosol during ER stress. (*A*) Schematic of the ER-targeted yemEos3.2 construct. (*B*) Microscopy images of WT cells expressing ER-targeted yemEos3.2, before and after photoconversion at both wavelengths (488 and 550 nm). (*C* and *D*) ER-targeted yemEos3.2 was first photoconverted by UV light in WT cells, and then images were taken (550 nm) after conversion for the indicated time points in the absence (*C*) or presence (*D*) of Tm.

for preexisting mEos3.2. Thus, the ER-mEos3.2 detected in the 573-nm channel (red) represents preexisting reporter, while newly synthesized ER-mEos3.2 will be detected in the 507-nm channel (green). In the absence of stress, ER-mEos3.2 localizes to the ER, both before and after photoconversion (Fig. 2 *B* and *C* and Movie S1). But when treated with Tm after photoconversion, ER-mEos3.2 (red) localized to the cytosol in a time course consistent with that seen for eroGFP reduction (Fig. 2*D* and Movie S2). Furthermore, we found that ER-mEos3.2 accumulates in the cytosol in its fluorescent (i.e., correctly folded) state for up to 8 h after Tm treatment without being degraded (Movie S3). Thus, remarkably, ER stress resulted in preexisting ER-mEos3.2 protein returning back from the ER to the cytosol in an intact, folded state (as with the two other reporters described above). We termed this retrograde trafficking process "ER protein reflux" and decided to study the phenomenon further through genetics.

Comprehensive Identification of Genes Affecting Reflux of eroGFP. What factors could promote the reflux of eroGFP (and ER-mEos3.2) already targeted to, residing in, and properly folded (i.e., fluorescent) in the ER back to the cytosol in an intact state? To identify genes mediating this reflux phenomenon, we integrated the eroGFP reporter into the *Saccharomyces cerevisiae* nonessential gene deletion collection (14) and the essential gene DAmP library (15) using synthetic genetic array techniques (*SI Appendix*, Fig. S3*A*) (16). Using high-throughput flow cytometry (17, 18), we measured the eroGFP ratios in ∼6,000 mutant strains during exposure to Tm and compared the ratios with untreated controls (Datasets S1 and S2). We observed a range of ratios, consistent with the idea that the mutants can modulate reflux of eroGFP during ER stress. To define hits, we fitted a curve to the difference between replicate measurements and obtained threshold eroGFP ratio values corresponding to $P < 0.001$ (*SI Appendix*, *Materials and Methods* and Fig. S3 *B*–*G*). After treatment with Tm, eroGFP ratios increased to a mean value of 0.57 in wild-type cells, normalized to untreated (Fig. 3*A* and Dataset S2). This value corresponds approximately to the eroGFP ratio of wild-type cells treated with 0.5 mM DTT (Fig. 1*B*). Exploiting the fact that this regime of Tm treatment caused

an intermediate (subcomplete) level of reduction (Fig. 1*B*), we could identify hundreds of mutants with eroGFP ratios that are both higher (sensitive hits) and lower (resistant hits) than the deflection experienced by wild-type cells (Fig. 3*A*).

In a previous genomic screen, basal UPR activity resulting from mutation of most nonessential genes in *S. cerevisiae* was comprehensively measured (19). Using these datasets, we compared each mutant's UPR activity with its eroGFP ratio under Tm-induced stress. Unexpectedly, we found that there is minimal global overlap between gene deletions that constitutively induce the UPR and those that significantly perturb eroGFP oxidation during Tm treatment (see Venn diagrams in Fig. 3*B*). However, when we examined mutant subsets grouped by their common molecular functions, we identified three subgroups in which correlations are evident between the two reporters (Fig. 3*B*). Mutants displaying both increased UPR activity and increased eroGFP ratios (compared with wild type) are found in quadrant I; these subgroups have mutations in genes encoding subunits of the ER membrane complex (EMC), components of the ER-associated degradation system, and activities needed for trafficking throughout the secretory pathway (*SI Appendix*, Fig. S3*H*). Mutants in quadrant IV display decreased eroGFP ratios despite increased UPR activity; these subgroups have mutations in genes encoding activities supporting N-linked glycosylation in the ER and many ER and cytosolic chaperones and cochaperones. Identification of quadrant IV mutant chaperone/cochaperone groups was unexpected, and will be addressed in the following section. The UPR-deficient mutants, *ire1*Δ and *hac1*Δ, had greater eroGFP ratio deflection than wild type upon Tm exposure [quadrant II—as we previously showed in real-time flow cytometry studies (6)], supporting the expectation that these mutants experience more ER stress relative to wild type because they cannot trigger a protective UPR.

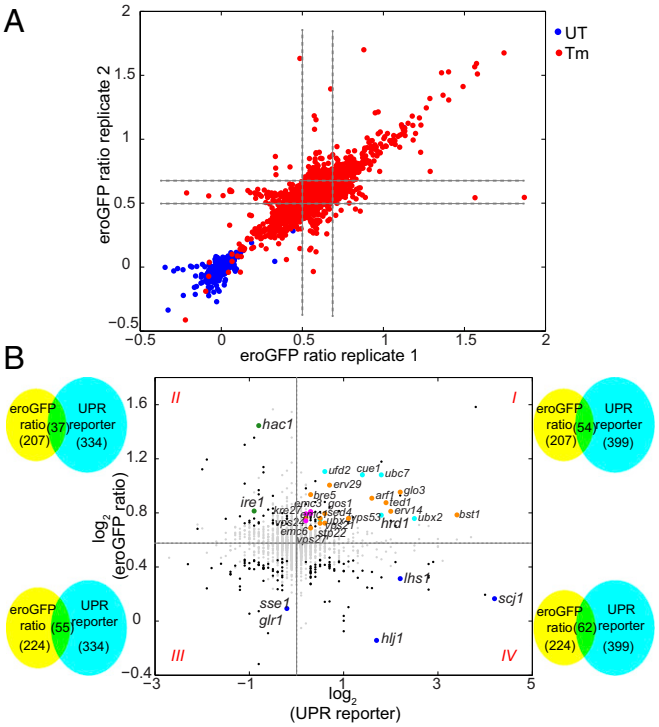

Fig. 3. Quantitative screen for genes whose deletion or down-regulation affects eroGFP oxidation. (*A*) Median eroGFP ratios of the deletion and DAmP libraries with and without Tm (6 μg/mL for 5 h). (*B*) Scatter plot of median eroGFP ratios after Tm treatment vs. UPR reporter levels for the nonessential yeast deletion library (19). The following gene categories are indicated by color: cyan (ERAD), orange (trafficking), magenta (EMC) (19), blue (ER-resident chaperones), and green (UPR). Venn diagrams indicate overlap for each quadrant.

Reflux of ER-Resident Proteins Requires Cytosolic and ER Chaperones. To identify components mediating ER protein reflux, we first focused on ERAD components, since many ERAD genes are up-regulated during ER stress (4) and their encoded products exert quality control by removing misfolded secretory proteins to the cytosol for subsequent ubiquitylation and degradation by the 26S proteasome. However, as mentioned above, genes associated with the canonical ERAD pathway were not among the resistant hits. Instead, several ERAD-defective mutants are found in quadrant I (increased eroGFP ratios during Tm treatment—i.e., sensitive hits) (Fig. 3*B* and Dataset S2). In *S. cerevisiae*, the membrane proteins HRD1 and DOA10 are the predominant ERAD ubiquitin-protein E3 ligases whose cytoplasmically oriented RING domains recruit distinct ubiquitin-conjugating enzymes to cause substrate ubiquitylation (20–23). Confirming the finding from the screen that these ERAD components are not required for ER protein reflux, we found that eroGFP refluxes to the cytosol after treatment with Tm in both single and double mutants of HRD1 and DOA10 (Fig. 4*A*). To follow the dynamics of the reflux process, we used ER-mEos3.2 and found that not only were HRD1 and DOA10 unnecessary for ER reporter reflux to the cytosol but that in the absence of these ERAD components, reflux even occurred in the absence of Tm, with some basal level of reporter seen in the cytosol in untreated cells, and more rapidly in the presence of Tm (Fig. 4 *A*–*E* and Movies S4 and S5).

In our previous study, we found that expressing the constitutively misfolded secretory protein CPY* under the Cup1 promoter in ERAD mutants increased the ratio of reduced eroGFP upon addition of copper (6). Here, we tested whether ER protein reflux could account for the increased eroGFP ratio that we had previously observed. To this end, we monitored the localization of the ER-targeted mEos3.2 in a *hrd1*Δ*doa10*Δ double-mutant strain that expresses CPY* under the Cup1 promoter. We found that in cells expressing CPY*, photoconverted ER-targeted mEos3.2 robustly localized to the cytosol and stayed fluorescent in the cytosol for up to 6 h after copper was added (Fig. 4 *F*–*I* and Movie S6).

In sum, it appeared that ER-to-cytosol reflux of eroGFP (or ER-mEos3.2) during ER stress not only does not rely on ERAD function but furthermore, mutations in many ERAD components, or the proteasome, appear to compensatorily increase the reflux process and recovery of intact reduced eroGFP in the cytosol (i.e., these are all sensitive hits with eroGFP ratios > WT). Moreover, in support of the notion that ER reflux may work in parallel with (or even substitute for) ERAD, the forced overexpression of CPY* was sufficient to cause spontaneous reflux of ER-targeted mEos3.2 in the *hrd1*Δ*doa10*Δ double mutant. Finally, supporting the notion that eroGFP reflux is not dependent on ERAD, eroGFP appeared to not be poly-ubiquitinated during Tm provision (unlike CPY*) (*SI Appendix*, Fig. S4 *A* and *B*).

Next, to identify and characterize genes that may mediate the ER protein reflux process, we focused on ER-resident proteins from our screen that showed minimal eroGFP ratio changes during Tm treatment (i.e., resistant hits in quadrant IV; Fig. 3*B*). Through this analysis, HLJ1, an ER-resident tail-anchored cochaperone, containing a cytosolically disposed DnaJ domain, stood out as the single, strongest resistant hit among ER-resident proteins. We confirmed that the *hlj1*Δ mutant did not alter eroGFP oxidation after Tm treatment (Fig. 5*A*). Furthermore, in *hlj1*Δ mutants, eroGFP remained in reticular structures that did not overlap with cytosolic tdTomato during Tm treatment, though a small fraction of eroGFP localized to the vacuole even under unstressed conditions (Fig. 5 *B* and *D*). As with eroGFP,

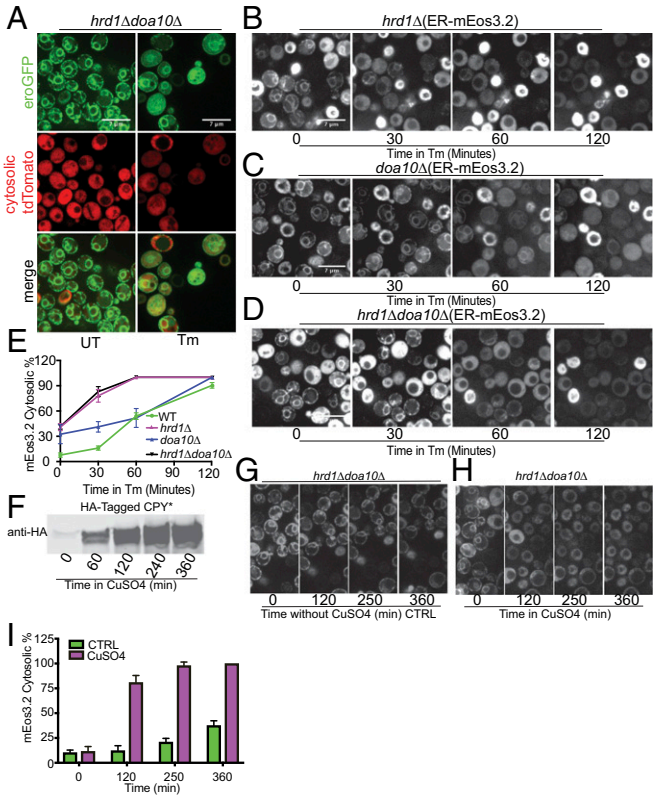

Fig. 4. ER protein reflux is not reliant on canonical ERAD machinery. (*A*) Confocal images for the *hrd1Δdoa10Δ* double mutant expressing eroGFP treated with Tm (6 μg/mL) for 2 h. (*B–D*) Confocal images for *hrd1Δ* (*B*), *doa10Δ* (*C*), and *hrd1Δdoa10Δ* double mutant (*D*) expressing the ER-targeted yemEos3.2 and treated with Tm for the indicated time points. (*E*) Quantification of images in *B–D* of *hrd1Δ*, *doa10Δ*, and *hrd1Δdoa10Δ* with ER-targeted yemEos3.2. Error bars represent SEM of two independent experiments. (*F*) Immunoblot (anti-HA) of protein extracts from wild-type cells expressing HA-tagged CPY* under the Cup1 promoter after addition of copper sulfate for the indicated time points. (*G* and *H*) Confocal microscopy images of *hrd1Δdoa10Δ* double-mutant cells expressing ER-targeted mEos3.2 and CPY* under the Cup1 promoter in the absence (*G*) and presence of copper sulfate (*H*) after photoconversion for the indicated time points. (*I*) Quantification of images of *hrd1Δdoa10Δ* with ER-targeted yemEos3.2 control or after $CuSO_4$ treatment. Error bars represent SEM of two independent experiments.

photoconverted (preexisting) ER-mEos3.2 remained localized to the ER in the *hlj1Δ* mutant upon Tm treatment (*SI Appendix*, Fig. S5 *A* and *B*). Thus, as predicted, the resistant hits from the genetic screen successfully identified a gene whose product promoted the reflux process. However, in each case, the combination of fluorescence microscopy and flow cytometry for the eroGFP ratio value needs to be compared. For example, a special exception for a resistant hit that leaves reflux unaffected is the *glr1Δ* glutathione oxidoreductase deletion mutant, in which Tm still caused eroGFP to reflux to the cytosol (as with WT) but without appreciably changing the eroGFP ratio from untreated (i.e., 0.09; Dataset S2). Glr1 is responsible for maintaining a reduced cytosol by converting oxidized to reduced glutathione (24, 25), and its absence even causes oxidation of cyto-roGFP (*SI Appendix*, Fig. S5 *C* and *D*).

In yeast, the ER-resident chaperone KAR2 acts as an anterograde molecular ratchet during translocation of secretory proteins through the Sec61 translocon. The binding of KAR2 to a translocating polypeptide on the luminal side of the Sec61 channel prevents it from moving backward (7). Successful protein translocation requires interaction between KAR2 and the Sec complex via the J domain of SEC63p (21, 26–31). Perhaps the resistant mutants identified from our screen may promote retrograde movement of eroGFP during ER stress-induced reflux. For instance, we found that besides HLJ1, mutations of genes encoding other ER and cytosolic chaperones, cochaperones, and nucleotide exchange factors (e.g., *lhs1Δ*, *kar2*-DAmP, sec66, and *sse1Δ*) also resisted eroGFP reduction and cytosolic relocalization upon Tm treatment (Fig. 3*B* and Dataset S2). Thus, we hypothesized that these chaperones and cochaperones may assist eroGFP reflux and should therefore bind this client protein during ER stress. To test this notion, we immunoprecipitated C-terminal FLAG-tagged HLJ1 in WT cells expressing eroGFP and found increasing interactions between HLJ1 and eroGFP over the time course of Tm treatment (Fig. 5*E*); this increase in the interaction between HLJ1 and eroGFP correlated with the kinetics of eroGFP protein reflux in these cells (*SI Appendix*, Fig. S1*D*).

A null mutation in SSE1 (also a resistant hit), which encodes a cytosolic nucleotide exchange factor and acts as a "holdase," also strongly resisted eroGFP reflux during ER stress (32–36) (Fig. 5*C*). Moreover, we found that eroGFP progressively interacts over time with FLAG-tagged SSE1 under Tm treatment in WT cells (Fig. 5*F*); this interaction between SSE1 and eroGFP became

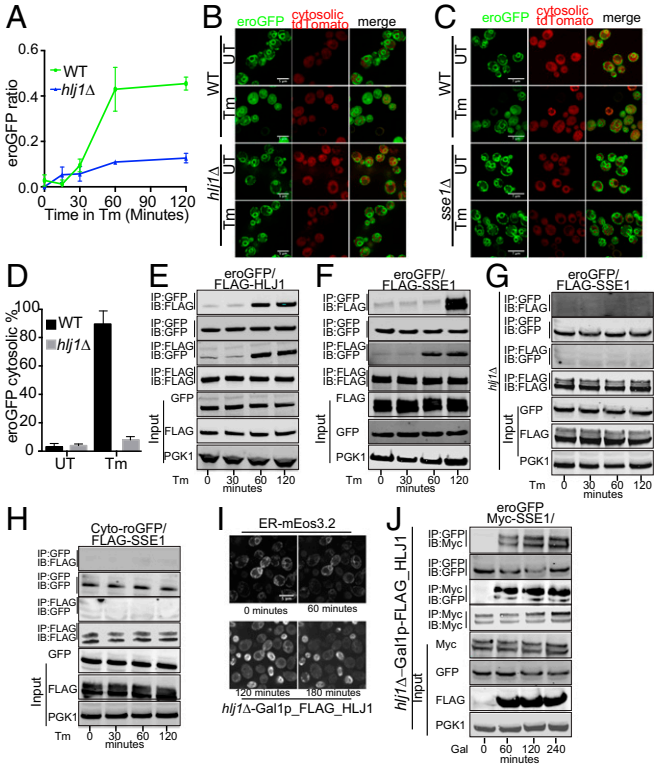

Fig. 5. Reflux of ER proteins requires HLJ1 and SSE1. (*A*) Time course of eroGFP ratios in wild-type and *hlj1Δ* cells expressing eroGFP treated with 6 μg/mL Tm. (*B*) Confocal images of eroGFP in wild-type and *hlj1Δ* treated with Tm (6 μg/mL) for 2 h. (*C*) Confocal images of WT and *sse1Δ* treated with Tm (6 μg/mL) for 2 h. (*D*) Quantification of WT and *hlj1Δ* images. Error bars represent SEM of two independent experiments. (*E* and *F*) Immunoprecipitation (IP) of C-terminal FLAG-tagged HLJ1 (*E*) or FLAG-tagged SSE1 (*F*) and eroGFP in WT cells after treatment with Tm (6 μg/mL). IB, immunoblotting. (*G*) Immunoprecipitation of C-terminal FLAG-tagged SSE1 and ER-targeted eroGFP in *hlj1Δ* cells. (*H*) Immunoprecipitation of C-terminal FLAG-tagged SSE1 and cytosolic roGFP in WT cells treated with Tm (6 μg/mL). (*I*) Confocal images of ER-targeted mEos3.2 in *hlj1Δ* cells overexpressing FLAG-tagged HLJ1 under the Gal1/10 promoter after shifting to galactose-containing media. (*J*) Immunoprecipitation of C-terminal Myc-tagged SSE1 and ER-targeted eroGFP in *hlj1Δ* cells overexpressing HLJ1 after shifting to galactose-containing media.

abrogated in *hlj1*Δ cells (Fig. 5*G*). Furthermore, to eliminate the possibility that SSE1 may interact with eroGFP after it has already translocated to the cytosol (i.e., in a nonreflux manner), we employed the cytosolic version of roGFP (cyto-roGFP) described above and did not observe an interaction between SSE1 and this cytosolic roGFP variant (Fig. 5*H*). Importantly, this last result supports the conclusion that under ER stress the reporter has to originate from inside the ER lumen to interact later with cytosolic SSE1.

Because all preceding data supported the notion that HLJ1 is necessary for ER protein reflux during ER stress, we next asked whether HLJ1 is sufficient to cause reflux of ER proteins to the cytosol upon forced expression. Because HLJ1 is lethal when constitutively overexpressed in *S. cerevisiae*, we placed a FLAG-tagged HLJ1 under the control of the inducible GAL1/10 promoter and followed its expression for several hours (*SI Appendix*, Fig. S5*E*). We found that 2 to 4 h after shifting cells to galactose a significant fraction of ER-targeted eroGFP spontaneously accumulated in the cytosol, without the need for exogenous ER stress agents (*SI Appendix*, Fig. S5*F*). To confirm the ER origin of the refluxed reporter, we expressed ER-targeted mEos3.2 in the inducible FLAG-HLJ1 strain and followed the reporter's fate during growth on galactose; at 3 h after the shift to galactose media, the majority of cells displayed a spontaneous cytosolic localization of the photoconverted mEos3.2 (Fig. 5*I*). Finally, we observed that in cells overexpressing HLJ1p there was an increased reciprocal physical interaction (through coimmunoprecipitation) between eroGFP and the cytosolic chaperone SSE1p, but without the need for exogenous ER stress agents (Fig. 5J). Thus, HLJ1p was both necessary and sufficient to promote ER reflux.

Finally, we inquired into the scope of the reflux process—that is, does it extend to other ER proteins (besides the FP reporters used in this study)? In theory, other ER-targeted proteins may also reflux to the cytosol during ER stress. To test this notion, we monitored the localization of ER endogenous protein disulfide isomerase (PDI1) and peptidyl-prolyl *cis–trans* isomerase (CPR5) during ER stress. Following treatment with Tm, we found that both CPR5 and PDI1 became progressively enriched over time in the cytosolic fraction (i.e., S100, the supernatant collected after the 100,000 × *g* ultracentrifugation) in WT cells, with similar kinetics to eroGFP, while the ER membrane protein Spf1 (predictably) remained in the membrane fraction (i.e., P100, the pellet generated from the 100,000 × *g* ultracentrifugation) (as with Hrd1-eroGFP) (Fig. 1). Importantly, in *hlj1*Δ cells, both CPR5 and PDI1 remained stably in the membrane fraction (as did eroGFP) (*SI Appendix*, Fig. S5*G*). Finally, applying the inducible ER stress regime of expressing the CPY* mutant using the CUP promoter in the *hrd1*Δ*doa10*Δ double mutant, we found increased recovery (compared with expression of CPY) of CPR5, PDI1, and eroGFP in the cytosolic fraction (*SI Appendix*, Fig. S5*H*).

To conclude our study, we also asked whether cells resistant to ER protein expulsion may perhaps be more susceptible to ER stress than wild-type cells. To this end, we performed a yeast viability assay by treating WT and *hlj1*Δ cells with Tm for 4 h and then spread the same optical density of cells on YPD plates and counted the viable colonies on the plate. We found that in this regime, WT cells were almost ∼75% viable, while in *hlj1*Δ and *sse1*Δ mutants only 53 and 50% of the cells were viable, respectively (*SI Appendix*, Fig. S5*I*). A plate sensitivity assay also confirmed that *hlj1*Δ and *sse1*Δ are more susceptible to ER stress (*SI Appendix*, Fig. S5*J*). These data were consistent with the possibility that blocking ER protein expulsion may cause yeast cells to become more sensitive to acute ER stress.

Discussion

In response to ER stress, several cellular stress response pathways, such as ERAD and the UPR, become activated to restore protein-folding homeostasis in the ER. Here, using a combination of fluorescence microscopy and high-throughput flow cytometry of yeast gene deletion libraries to measure fluorescent changes in an ER-targeted redox-sensitive GFP, we identify a cellular stress response pathway in which ER-resident proteins are removed in an intact state back into the cytosol through a chaperone-mediated manner. We have termed this process ER protein reflux.

We had originally adapted eroGFP to track ambient redox state as a proxy measure of ER physiological health, and previously shown that reduction of the normally oxidized eroGFP occurred in individual cells (wild type and a few select mutants) during ER stress induced by inhibiting N-linked glycosylation, inositol deprivation (in UPR mutants), and expressing misfolded secretory proteins (e.g., CPY*) (6). Here we have confirmed our previous conclusion that reduction of eroGFP occurs after its translocation and maturation in the ER (6) (i.e., in a preexisting, ER-resident reporter) by using an eroGFP variant in which an N-linked glycosylation signal is engineered at the C terminus of the reporter (called eroGFP-Glyc). When expressed through a GAL 1/10 inducible system in which new transcription and translation are shut off through application of glucose followed by induction of ER stress, preexisting eroGFP-Glyc became deglycosylated in the cytosol and eroGFP-Glyc's asparagine-linked glycan converted into an aspartate residue as measured using 2D electrophoresis and mass spectrometry. In direct support of these biochemical data, we observed, using live-cell imaging, a photoconverted ER-resident mEos3.2 reflux into the cytosol during ER stress, with similar kinetics to the reduction of eroGFP observed during similar modes of ER stress.

By measuring eroGFP ratios in yeast gene deletion libraries using high-throughput flow cytometry, we first identified both sensitive and resistant mutants that precisely change eroGFP oxidation levels to varying degrees during ER stress. eroGFP ratio changes in the mutants showed limited overlap with changes measured by a UPR reporter, validating the use—at the genomic scale—of the utility of a redox-responsive reporter to provide orthogonal information about a physiological secretory pathway function to a corrective signaling pathway (the UPR). Then, by validating the hits from the screen using fluorescence microscopy, we uncovered the chaperone-mediated basis of the ER protein reflux phenomenon. This reflux phenomenon was missed in our prior eroGFP work (that only utilized flow cytometry of a small group of mutants) in which we had proposed an unnecessarily constrained interpretation of eroGFP oxidation changes occurring within the ER (6). The central feature of ER protein reflux appears to be that soluble, folded proteins (i.e., fluorescent in the case of the reporters) are removed from the ER without becoming degraded (unlike in the ERAD process). Furthermore, upon their reflux to the cytosol, the preexisting reporters that originated from the ER remain fluorescent (i.e., folded) for at least 8 h. Further distinguishing reflux from ERAD, we found that eroGFP, eroGFP-Glyc, ER-mEos3.2, and endogenous ER proteins are returned to the cytosol in the absence of the canonical ERAD-associated E3 ubiquitin-protein ligases HRD1 and DOA10.

ER reflux, however, is strikingly abrogated in the absence of HLJ1, a tail-anchored ER membrane cochaperone with a cytosolically disposed J domain. HLJ1 is known to have overlapping roles with another cochaperone containing a cytosolic J domain, YDJ1, in promoting the removal and ubiquitin-dependent degradation of the ER membrane protein CFTR (37). Intriguingly, *ydj1*Δ is a sensitive hit in our screen (Dataset S2), supporting the notion that it does not play an overlapping role with YDJ1 in reflux. It is thus conceivable that HLJ1 has an auxiliary role(s) in ER protein quality control beyond those previously ascribed to it (e.g., through mediating reflux). More generally, besides *hlj1*Δ, mutations in other ER-resident chaperones and cochaperones (e.g., *lhs1*Δ, *kar2*-DAmP, *scj1*Δ) (Fig. 3*B*, quadrant IV and Dataset S2) also resist eroGFP oxidation changes during ER stress to varying degrees. Thus, these gene products may also

play critical roles in mediating and regulating ER protein reflux; future investigations into the functions of these gene products may provide a more comprehensive understanding of ER protein reflux. For instance, besides HLJ1, we found notably that cytosolic SSE1, an Hsp110 chaperone/nucleotide exchange factor/holdase, which also emerged from the resistant hits in our screen, can bind eroGFP in an HLJ1-dependent manner under ER stress (and, importantly, only if the reporter is first targeted to the ER rather than originating from the cytosol).

Finally, we note that we do not yet fully understand how folded ER-resident proteins can reemerge in a folded state (i.e., fluorescent in the case of eroGFP, eroGFP-Glyc, and mEos3.2) in the cytosol. While it is conceivable that reflux substrates stay folded during this retrograde transit across the ER membrane (perhaps transiting through an ER channel), no obvious candidate genes meeting the expected criteria of a putative channel were identified as (resistant) hits in our screens. Therefore, while remaining agnostic to the involvement of a putative channel, we suggest that a relay shuttle of ER-resident and cytosolic chaperones (e.g., KAR2, HLJ1, SSE1) may allow for partial unfolding in the ER, transit across the ER, and refolding in the cytosol of ER luminal proteins during ER stress. Such a process is intriguingly reminiscent of, but directionally opposite, that of the chaperone-assisted molecular ratchet that promotes translocation of nascent secretory proteins (7). Furthermore, putative functional homologs of HLJ1 in humans, DnaJB12 and DnaJB14, which were shown to mediate retrograde trafficking/entry into the cytosol from the ER of nonenveloped viruses (38), may also promote ER stress-induced protein reflux in mammalian cells. In this speculative view, the ER reflux machinery may perhaps be usurped by some viruses to gain entry to the cytosol.

While the larger scope of ER reflux remains to be defined, the process could conceivably extend to many endogenous ER-resident proteins (and maturing secretory cargo). Indeed, our finding that PDI1 and CPR5 proteins are recovered (through an HLJ1-dependent mechanism) in the cytosol during ER stress is consistent with the possibility that these proteins are also reflux substrates (and provides an explanation for previous enigmatic reports of how ER chaperones could be found in the cytosol) (39–41). Physiologically, it is conceivable that ER protein reflux, by clearing the ER of luminal proteins during ER stress, may have an adaptive benefit and may work in parallel with other ER protein quality control mechanisms such as ERAD and protein translocational attenuation, referred to as preemptive quality control (11). Indeed, the decreased viability of *sse1* and *hlj1* mutants under ER stress is consistent with this possibility. It is also conceivable that ER protein reflux may be integrated into the binary cell-fate decisions made by cells of higher eukaryotes once ER stress levels reach critical thresholds. Future studies will address such mechanistic and physiological questions.

Materials and Methods

Plasmid Construction. eroGFP-Glyc was constructed using the QuikChange Lightning Kit (Agilent Technologies). The glycosylation site was engineered in the second residue of the 9-amino acid linker between the C terminus of GFP and the HDEL retrieval sequence. eroGFPND was also constructed using the QuikChange Lightning Kit to change the asparagine in eroGFP-Glyc to an aspartate. Hrd3-eroGFP was constructed using synthetic DNA from GeneArt (Life Technologies) containing eroGFP followed by residues 767 to 833 of HRD3. ER-yemEos3.2 was constructed by PCR amplification of yemEos3.2 (a gift from Erik Snapp, Janelia Research Campus, Ashburn, VA) using forward oligos containing the first 20 amino acids of yemEos3.2 and reverse oligos of the last 20 amino acids with addition of an HDEL sequence. This construct was then cloned in pRS416 carrying the Kar2 signal peptide by BamHI and XbaI. HLJ1 and SSE1 were PCR-tagged in the chromosome under their native promoter with either a 3×FLAG tag or 3×HA tag using pFA6a-3×FLAG-NAT or pFA6a-3×HA-His3MX6 plasmids.

High-Throughput Flow Cytometry. For all growth conditions described below, yeast strains were grown in 80 μL SD complete media supplemented with myo-inositol (Sigma-Aldrich) at 100 μg/mL. For tunicamycin experiments, Tm was added to the media at 6 μg/mL. Strains were inoculated from 384-colony agar plates to 384-well liquid cultures using a RoToR HDA robot (Singer Instruments). The cultures were grown for 36 h to saturation in a DTS-4 microplate thermoshaker (Appropriate Technical Resources). They were then diluted 1:400 using a Biomek liquid-handling robot (Beckman Coulter) and grown to mid-log phase for 10 h, after which they were diluted 1:10 into media with or without Tm. After 5 h of growth, cultures were loaded on a Becton Dickinson High Throughput Sampler, which injected cells from each well into an LSR II flow cytometer (Becton Dickinson). eroGFP fluorescence was measured according to ref. 6.

Light Microscopy. Yeast were imaged as previously described (6) with the exception that a 561-nm laser line was used to excite tdTomato. Cells carrying ER-yemEos3.2 were grown to mid-log phase and then immobilized on Con A glass bottom dishes (Mattek Corporation). Cells then were imaged using the 488-nm channel followed by 1 min with DAPI for photoconversion. Tm was then added and cells were imaged for 2 h using an inverted Nikon Ti high-speed wide-field microscope equipped with a CSU-W1 spinning disk confocal with Borealis upgrade (Andor). All other images were captured using a spinning disk confocal microscope at the Nikon Imaging Center (University of California, San Francisco).

Immunoblots and Immunoprecipitation. For yeast immunoprecipitation studies, we followed the exact protocol as in ref. 42 with one modification: After collecting the cells, proteins were extracted by disrupting the cells twice with glass beads in the lysis buffer for 45 s in a TissueLyser II (QIAGEN). Immunoblots were performed as previously described (6). Antibodies used included rabbit anti-GFP, mouse anti-PGK1 (Thermo Fisher), monoclonal anti-FLAG M2 antibody (Sigma-Aldrich), and anti-HA tag antibody (Ptglabs). Antibody binding was detected by using near-infrared dye-conjugated secondary antibodies (LI-COR) on the LI-COR Odyssey scanner.

Note Added in Proof. Prior to peer review, ER protein reflux was independently reported on the bioRxiv preprint server by our group (43) and Erik Snapp's group (44) on March 12, 2019.

ACKNOWLEDGMENTS. We thank Erik Snapp for the yemEos3.2 plasmid, stimulating discussions, and exchanging data; Jeff Brodsky for providing the *hrd1Δdoa10Δ* double-mutant strain; and David Breslow for the cytosolic tdTomato plasmid. A.I. was supported by a JDRF postdoctoral fellowship, and P.I.M. was supported by a National Science Foundation Graduate Research Fellowship and a Ruth L. Kirschstein National Research Service Award. F.R.P. was supported by grants from the NIH (Director's New Innovator Award DP2 OD001925 and R01DK095306) and a Career Award in the Biomedical Sciences from the Burroughs Wellcome Foundation.

1. Rapoport TA (2007) Protein translocation across the eukaryotic endoplasmic reticulum and bacterial plasma membranes. *Nature* 450:663–669.
2. van Anken E, Braakman I (2005) Versatility of the endoplasmic reticulum protein folding factory. *Crit Rev Biochem Mol Biol* 40:191–228.
3. Vembar SS, Brodsky JL (2008) One step at a time: Endoplasmic reticulum-associated degradation. *Nat Rev Mol Cell Biol* 9:944–957.
4. Travers KJ, et al. (2000) Functional and genomic analyses reveal an essential coordination between the unfolded protein response and ER-associated degradation. *Cell* 101:249–258.
5. Rutkowski DT, et al. (2006) Adaptation to ER stress is mediated by differential stabilities of pro-survival and pro-apoptotic mRNAs and proteins. *PLoS Biol* 4:e374.
6. Merksamer PI, Trusina A, Papa FR (2008) Real-time redox measurements during endoplasmic reticulum stress reveal interlinked protein folding functions. *Cell* 135:933–947.
7. Matlack KE, Misselwitz B, Plath K, Rapoport TA (1999) BiP acts as a molecular ratchet during posttranslational transport of prepro-alpha factor across the ER membrane. *Cell* 97:553–564.
8. Misselwitz B, Staeck O, Matlack KE, Rapoport TA (1999) Interaction of BiP with the J-domain of the Sec63p component of the endoplasmic reticulum protein translocation complex. *J Biol Chem* 274:20110–20115.
9. Hanson GT, et al. (2004) Investigating mitochondrial redox potential with redox-sensitive green fluorescent protein indicators. *J Biol Chem* 279:13044–13053.
10. Rubio C, et al. (2011) Homeostatic adaptation to endoplasmic reticulum stress depends on Ire1 kinase activity. *J Cell Biol* 193:171–184.
11. Kang SW, et al. (2006) Substrate-specific translocational attenuation during ER stress defines a pre-emptive quality control pathway. *Cell* 127:999–1013.
12. Suzuki T, Park H, Lennarz WJ (2002) Cytoplasmic peptide:N-glycanase (PNGase) in eukaryotic cells: Occurrence, primary structure, and potential functions. *FASEB J* 16:635–641.
13. Zhang M, et al. (2012) Rational design of true monomeric and bright photoactivatable fluorescent proteins. *Nat Methods* 9:727–729.

14. Giaever G, et al. (2002) Functional profiling of the *Saccharomyces cerevisiae* genome. *Nature* 418:387–391.
15. Breslow DK, et al. (2008) A comprehensive strategy enabling high-resolution functional analysis of the yeast genome. *Nat Methods* 5:711–718.
16. Tong AH, et al. (2001) Systematic genetic analysis with ordered arrays of yeast deletion mutants. *Science* 294:2364–2368.
17. Newman JR, et al. (2006) Single-cell proteomic analysis of *S. cerevisiae* reveals the architecture of biological noise. *Nature* 441:840–846.
18. Hanna J, Finley D (2007) A proteasome for all occasions. *FEBS Lett* 581:2854–2861.
19. Jonikas MC, et al. (2009) Comprehensive characterization of genes required for protein folding in the endoplasmic reticulum. *Science* 323:1693–1697.
20. Carvalho P, Goder V, Rapoport TA (2006) Distinct ubiquitin-ligase complexes define convergent pathways for the degradation of ER proteins. *Cell* 126:361–373.
21. Bays NW, Gardner RG, Seelig LP, Joazeiro CA, Hampton RY (2001) Hrd1p/Der3p is a membrane-anchored ubiquitin ligase required for ER-associated degradation. *Nat Cell Biol* 3:24–29.
22. Hampton RY, Gardner RG, Rine J (1996) Role of 26S proteasome and HRD genes in the degradation of 3-hydroxy-3-methylglutaryl-CoA reductase, an integral endoplasmic reticulum membrane protein. *Mol Biol Cell* 7:2029–2044.
23. Ravid T, Kreft SG, Hochstrasser M (2006) Membrane and soluble substrates of the Doa10 ubiquitin ligase are degraded by distinct pathways. *EMBO J* 25:533–543.
24. Kojer K, et al. (2012) Glutathione redox potential in the mitochondrial intermembrane space is linked to the cytosol and impacts the Mia40 redox state. *EMBO J* 31:3169–3182.
25. Morgan B, Sobotta MC, Dick TP (2011) Measuring E(GSH) and H_2O_2 with roGFP2-based redox probes. *Free Radic Biol Med* 51:1943–1951.
26. Brodsky JL, Schekman R (1993) A Sec63p-BiP complex from yeast is required for protein translocation in a reconstituted proteoliposome. *J Cell Biol* 123:1355–1363.
27. Corsi AK, Schekman R (1997) The lumenal domain of Sec63p stimulates the ATPase activity of BiP and mediates BiP recruitment to the translocon in *Saccharomyces cerevisiae*. *J Cell Biol* 137:1483–1493.
28. Lyman SK, Schekman R (1995) Interaction between BiP and Sec63p is required for the completion of protein translocation into the ER of *Saccharomyces cerevisiae*. *J Cell Biol* 131:1163–1171.
29. Matlack KE, Plath K, Misselwitz B, Rapoport TA (1997) Protein transport by purified yeast Sec complex and Kar2p without membranes. *Science* 277:938–941.
30. Sadler I, et al. (1989) A yeast gene important for protein assembly into the endoplasmic reticulum and the nucleus has homology to DnaJ, an *Escherichia coli* heat shock protein. *J Cell Biol* 109:2665–2675.
31. Sanders SL, Whitfield KM, Vogel JP, Rose MD, Schekman RW (1992) Sec61p and BiP directly facilitate polypeptide translocation into the ER. *Cell* 69:353–365.
32. Dragovic Z, Broadley SA, Shomura Y, Bracher A, Hartl FU (2006) Molecular chaperones of the Hsp110 family act as nucleotide exchange factors of Hsp70s. *EMBO J* 25:2519–2528.
33. Oh HJ, Easton D, Murawski M, Kaneko Y, Subjeck JR (1999) The chaperoning activity of hsp110. Identification of functional domains by use of targeted deletions. *J Biol Chem* 274:15712–15718.
34. Oh HJ, Chen X, Subjeck JR (1997) Hsp110 protects heat-denatured proteins and confers cellular thermoresistance. *J Biol Chem* 272:31636–31640.
35. Shaner L, Sousa R, Morano KA (2006) Characterization of Hsp70 binding and nucleotide exchange by the yeast Hsp110 chaperone Sse1. *Biochemistry* 45:15075–15084.
36. Mukai H, et al. (1993) Isolation and characterization of SSE1 and SSE2, new members of the yeast HSP70 multigene family. *Gene* 132:57–66.
37. Youker RT, Walsh P, Beilharz T, Lithgow T, Brodsky JL (2004) Distinct roles for the Hsp40 and Hsp90 molecular chaperones during cystic fibrosis transmembrane conductance regulator degradation in yeast. *Mol Biol Cell* 15:4787–4797.
38. Walczak CP, Ravindran MS, Inoue T, Tsai B (2014) A cytosolic chaperone complexes with dynamic membrane J-proteins and mobilizes a nonenveloped virus out of the endoplasmic reticulum. *PLoS Pathog* 10:e1004007.
39. Turano C, Coppari S, Altieri F, Ferraro A (2002) Proteins of the PDI family: Unpredicted non-ER locations and functions. *J Cell Physiol* 193:154–163.
40. Liu Z, et al. (2017) Effect of subcellular translocation of protein disulfide isomerase on tetrachlorobenzoquinone-induced signaling shift from endoplasmic reticulum stress to apoptosis. *Chem Res Toxicol* 30:1804–1814.
41. Yoshimori T, et al. (1990) Protein disulfide-isomerase in rat exocrine pancreatic cells is exported from the endoplasmic reticulum despite possessing the retention signal. *J Biol Chem* 265:15984–15990.
42. Gerace E, Moazed D (2014) Coimmunoprecipitation of proteins from yeast. *Methods Enzymol* 541:13–26.
43. Igbaria A, et al. (2019) Chaperone-mediated reflux of secretory proteins to the cytosol during endoplasmic reticulum stress. bioRxiv:562306. Preprint, posted March 12, 2019.
44. Lajoie P, Snapp EL (2019) Size-dependent secretory protein reflux into the cytosol in association with acute endoplasmic reticulum stress. bioRxiv:573428. Preprint, posted March 12, 2019.

SUPPLEMENTARY MATERIALS AND METHODS

Immunofluorescence:

Cells were grown to mid-log phase, collected by centrifugation at 3000rpm, then resuspended in 1mL of 4% paraformaldehyde solution for 30 minutes at room temperature. Cells were then centrifuged again and the pellet washed twice with 5mL of KS buffer (0.1 M KPO4/1.2 M sorbitol) before resuspending again in KS buffer. After fixation, spheroplasts were generated using 20T zymolyase and resuspended again in KS buffer. Slides were washed with cold acetone and then treated with 0.1%-polylysine before adding spheroplasts; slides were then washed and blocked with PBS-BSA for 30 minutes. Slides were incubated with the primary antibody overnight, then washed three times with PBS-BSA. Secondary antibodies were prepared in PBS-BSA and slides were incubated with the secondary antibodies for 2hrs before washing again with PBS-BSA. Slides were then mounted and sealed with nail polish.

Quantitative Real-Time PCR

RNA was isolated from whole cells using Qiagen RNeasy kit. 1μg total RNA was reverse transcribed using the QuantiTect Reverse Transcription Kit (Qiagen) and amplified using the StepOnePlus Real-Time PCR System (Applied Biosystems) with SYBR green. Thermal cycles were: 5 min at 95 °C, 40 cycles of 15 s at 95 °C, 30 s at 60 °C. Gene expression levels were normalized to PGK1. Primers used for Q-PCR were as follows: GFP: 5’-acaagcagaagaacggcatc-3’ and 5’-gcaggtgctcaggtagtggt-3’; PGK1: 5’-ctcactcttctatggtcggtttc-3’ and 5’-gagaacccaaccagaccatt-3’.

Subcellular Fractionation

Yeast organelles were fractionated using ultracentrifugation according to the protocol described in [1].

Estimating the fraction of newly synthesized eroGFP-Glyc

The time evolution of the eroGFP translation rate (m) and the concentration of eroGFP protein (P) were estimated from a two-step transcription-translation model:

$$\frac{dm}{dt} = -\frac{m}{T_M}$$

$$\frac{dP}{dt} = -\frac{\ln(2)}{T_P}(m - P)$$

m and P are normalized to their steady state levels in galactose conditions and are thus unitless variables. T_M, defined as the half-life of the eroGFP translation rate, was estimated from the pulse-label data. $\ln(2)/T_P$ is the half-life of eroGFP proteins that decay due to dilution from cell division. T_P is set to 120 min, which corresponds to the doubling time of yeast in SD media.

Mass Spectrometry Analysis

Immunoprecipitated FLAG-eroGFP-Glyc was purified by gel electrophoresis and subjected to in-gel trypsin digestion. Gel bands were diced and washed three times with 25 mM NH_4HCO_3/50% ACN, and evaporated to dryness. Cysteines were reduced by incubation with 10 mM DTT in 25 mM NH_4HCO_3 at 56°C for 1 hour, and free sulfhydryl groups were alkylated by incubation with 55 mM iodoacetamide for 45 minutes at room temperature. Gel pieces were washed twice with 25 mM NH_4HCO_3/50% ACN and evaporated to dryness. Gel pieces were rehydrated with 12.5 ng/μL trypsin in 25 mM

NH_4HCO_3 and incubated at 37°C overnight. The supernatant was removed and combined with two extractions with 50% ACN/5% formic acid. The combined supernatant was subjected to concentration on C18 ZipTips (Millipore) according to the manufacturer's specifications. Following evaporation, samples were resuspended in 0.1% formic acid for liquid chromatography and mass spectrometry (LC-MS/MS) analysis.

Digested peptide mixtures were analyzed in technical duplicate on a Thermo Scientific LTQ Orbitrap Elite mass spectrometry system equipped with a Proxeon Easy nLC 1000 ultra high-pressure liquid chromatography and autosampler system. Samples were injected onto a C18 column (25 cm x 75 um I.D. packed with ReproSil Pur C18 AQ 1.9 um particles) in 0.1% formic acid and then subjected to a 2-hours gradient from 0.1% formic acid to 30% ACN/0.1% formic acid. The mass spectrometer collected data in a data-dependent fashion, collecting one full scan in the Orbitrap at 120,000 resolution followed by 20 collision-induced dissociation MS/MS scans in the dual linear ion trap for the 20 most intense peaks from the full scan. Dynamic exclusion was enabled for 30 seconds with a repeat count of 1. Charge state screening was employed to reject analysis of singly charged species or species for which a charge could not be assigned. Extracted ion chromatograms for peptides of interest were generated using the Thermo Scientific XCalibur QualBrowser software package.

SUPPLEMENTARY FIGURE LEGENDS

Figure S1. ER-targeted eroGFP re-localizes to the cytosol during ER stress

(A) Time course of eroGFP ratio changes in WT cells upon exposure to DTT (blue) or Tm (red).

(B) eroGFP redox state in WT cells treated with Tm (6μg/mL) or DTT (1mM) for the indicated time points. Extracts were treated with NEM, resolved on non-reducing SDS-PAGE, and immunoblotted against GFP.

(C) Quantification of reduced eroGFP(red) percentage in WT cells treated with either Tm or DTT, ratios calculated from a non-reducing SDS-PAGE after alkylating the protein lysates with NEM for 30 minutes.

(D) Confocal images of wild-type cells expressing eroGFP and cytosolic tdTomato treated with Tm (6μg/mL) for the indicated time points.

Figure S2. Pre-existing eroGFP-Glyc is refluxed from the ER during ER stress.

(A) Schematic of eroGFP-Glyc. An *N*-linked protein glycosylation recognition sequence was inserted into the 9 amino acid linker between eroGFP and the HDEL retrieval sequence.

(B) Immunoblot (anti-GFP) of protein extracts from wild-type cells expressing eroGFP and eroGFP-Glyc.

(C) Schematic of FLAG-tagged GAL1-eroGFP-Glyc (top) and qPCR to determine relative eroGFP-Glyc mRNA levels. Cells were grown on Galactose for 4hrs, then shifted to glucose; time 0 indicates glucose addition.

(D) Pulse-label for wild-type cells expressing FLAG-tagged GAL1-eroGFPGlyc treated according to (B).

(E) Half-life of the FLAG-tagged eroGFP-Glyc translation rate (τ_M = 82min) is calculated by fitting an exponential decay curve, $e(-t/\tau_M)$, to the pulse-label data. The solid line represents the curve fit and the dashed lines represent 99% confidence bounds.

(F) The fraction of newly synthesized FLAG-tagged eroGFP-Glyc is estimated from a two-step transcription/translation model (see Methods).

(G) Confocal microscopy for eroGFP-Glyc. Cells were treated with galactose for 4hrs and then shifted to glucose containing media. After 2hrs on glucose, Tm was added for an additional 2 hrs.

(H) Two-dimensional gel electrophoresis followed by western blot of GAL1-eroGFP-Glyc for the indicated condition. FLAG-tagged eroGFP-ND indicates the GAL1-eroGFP-Glyc N to D point mutant. Duplicated blots are shown in the vertical and horizontal directions to aid visualization/alignment in both dimensions.

(I) Ratios of aspartate to asparagine at the position marked by * for cytosolic roGFP-Glyc (croGFP) and eroGFP-Glyc treated with Tm or PNGase where indicated.

Figure S3. Experimental Design and Analysis for the eroGFP screen.

(A) Schematic of mating strategy used to generate the eroGFP expressing gene libraries using the Synthetic Genetic Array strategy (Tong et al, 2001).

(B and C) Histograms of the differences between eroGFP replicate measurements for untreated and tunicamycin treated samples respectively

(D and E) Fit of the histograms from B and C modeled as the sum of two Gaussian distributions according to [2]. The fitted lines are in orange overlaid over the histograms from B and C.

(F and G) Histograms of the mean data for untreated and tunicamycin treated samples respectively in green overlaid over the histograms described in D-E.

(H) Enrichment of Gene Ontology terms ($P<0.001$) for the indicated ER functions.

Figure S4. ER protein reflux is not reliant on canonical ERAD machinery.

(A) Immunoprecipitation (IP) using anti-GFP antibody of extracts from wild-type cells treated with tunicamycin (or untreated) in the (presence/absence) of MG132, followed by immunoblot analysis with anti-ubiquitin (Ub) and anti-GFP antibodies.
(B) Immunoprecipitation (IP) using anti-HA antibody of extracts from wild-type cells expressing HA-tagged-CPY* treated with tunicamycin (or untreated) in the (presence/absence) of MG132, followed by immunoblot analysis with anti-ubiquitin (Ub) and anti-HA antibodies.

*Heavy chain

Figure S5. Reflux of ER proteins requires HLJ1

(A) ER targeted yemEos3.2 was first converted by UV in *hlj1*Δ cells and then cells were treated with Tm (6µg/mL). Images (550nm) were taken exactly after Tm addition and 120 minutes after treatment.

(B) Quantification of *hlj1*Δ images with ER- targeted mEos3.2.

(C) Confocal images for *glr1*Δ treated with Tm (6µg/mL) for 2hrs.

(D) Cyto-roGFP redox state in WT, *hlj1*Δ and *glr1*Δ cells treated with (6µg/mL) Tm. Protein extracts were treated with NEM, resolved on non-reducing SDS-PAGE, and immunoblotted against GFP.

(E) Immunoblot (anti-FLAG) of protein extracts from *hlj1*Δ cells overexpressing FLAG

tagged HLJ1 after induction with galactose for the indicated time points.

(F) Confocal images for *hlj1*Δ cells overexpressing WT-HLJ1 and expressing the ER-targeted mEos3.2 after shifting to Galactose containing media for the indicated time points.

(G) Subcellular protein fractionation of Myc-CPR5, PDI1 and eroGFP in WT, and *hlj1*Δ cells treated with Tm.

(H) Subcellular protein fractionation of CPR5, PDI1, and eroGFP in the ERAD double mutant (*hrd1*Δ *doa10*Δ) expressing either CPY or CPY* under the conditional promoter CUP1 (-/+) 200μM copper sulfate (CuSO4).

(I) Viability assay after Tm challenge for 4 hours in WT, *hlj1*Δ and *sse1*Δ cells.

(J) Plate sensitivity assay of WT, *hlj1*Δ and *sse1*Δ cells on Tm containing agar plates.

Movie S1: ER-targeted mEos3.2 in untreated WT cells followed for 120 minutes after photoconversion by a UV pulse.

Movie S2: ER-targeted mEos3.2 in Tm-treated WT cells followed for 120 minutes after photoconversion by a UV pulse.

Movie S3: ER-targeted mEos3.2 in Tm-treated WT cells followed for 8hours after photoconversion by a UV pulse.

Movie S4: ER-targeted mEos3.2 in Tm-treated WT cells followed for 120 minutes after photoconversion by a UV pulse.

Movie S5: ER-targeted mEos3.2 in Tm-treated *hrd1*Δ*doa10*Δ cells followed for 120 minutes after photoconversion by a UV pulse.

Movie S6: ER-targeted mEos3.2 in *hrd1*Δ*doa10*Δ cells expressing CPY* after addition of copper.

1. Rieder, S.E. and S.D. Emr, *Isolation of subcellular fractions from the yeast Saccharomyces cerevisiae.* Curr Protoc Cell Biol, 2001. **Chapter 3**: p. Unit 3 8.
2. Breslow, D.K., et al., *A comprehensive strategy enabling high-resolution functional analysis of the yeast genome.* Nat Methods, 2008. **5**(8): p. 711-8.

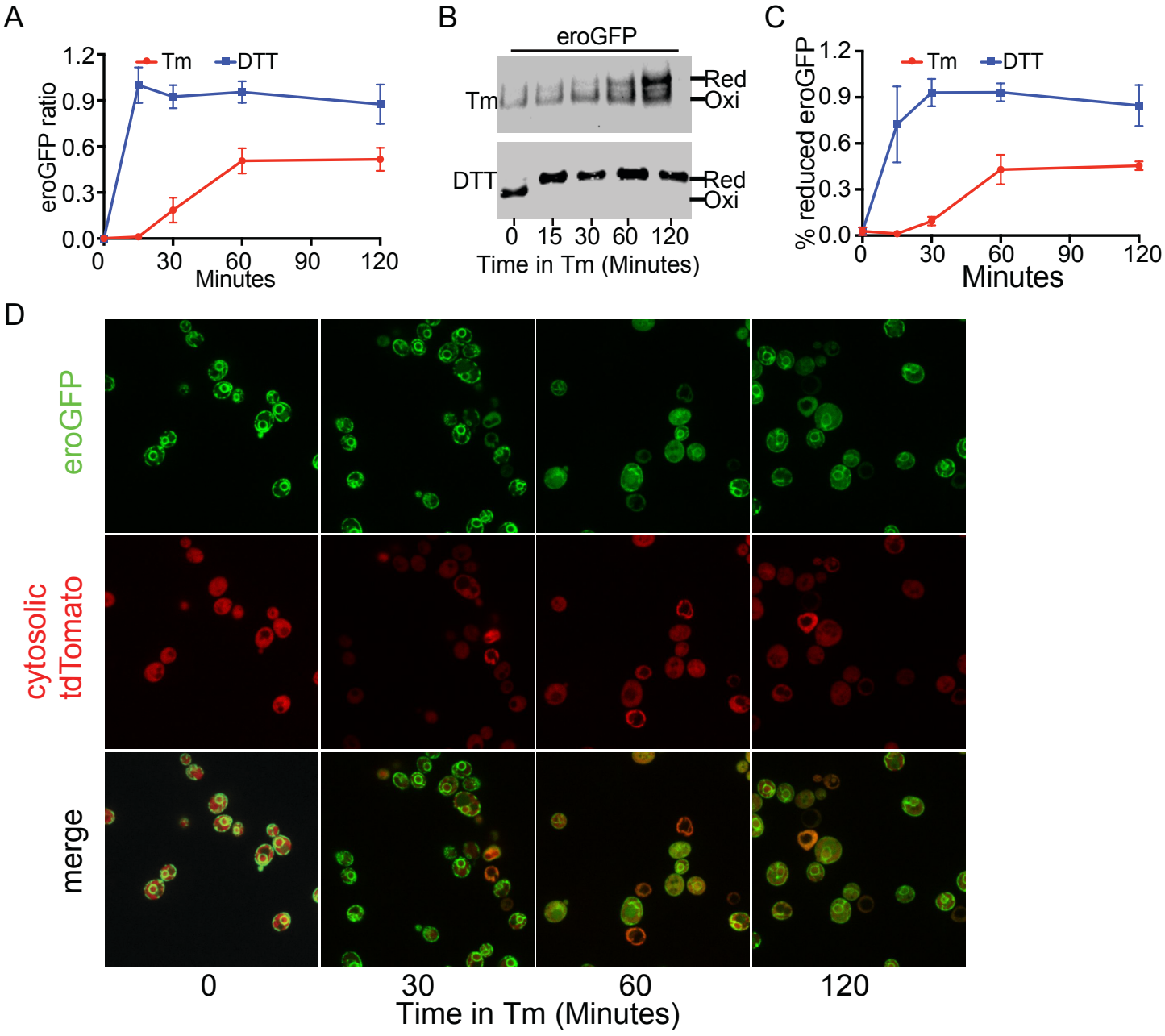

Igbaria et al Figure S1

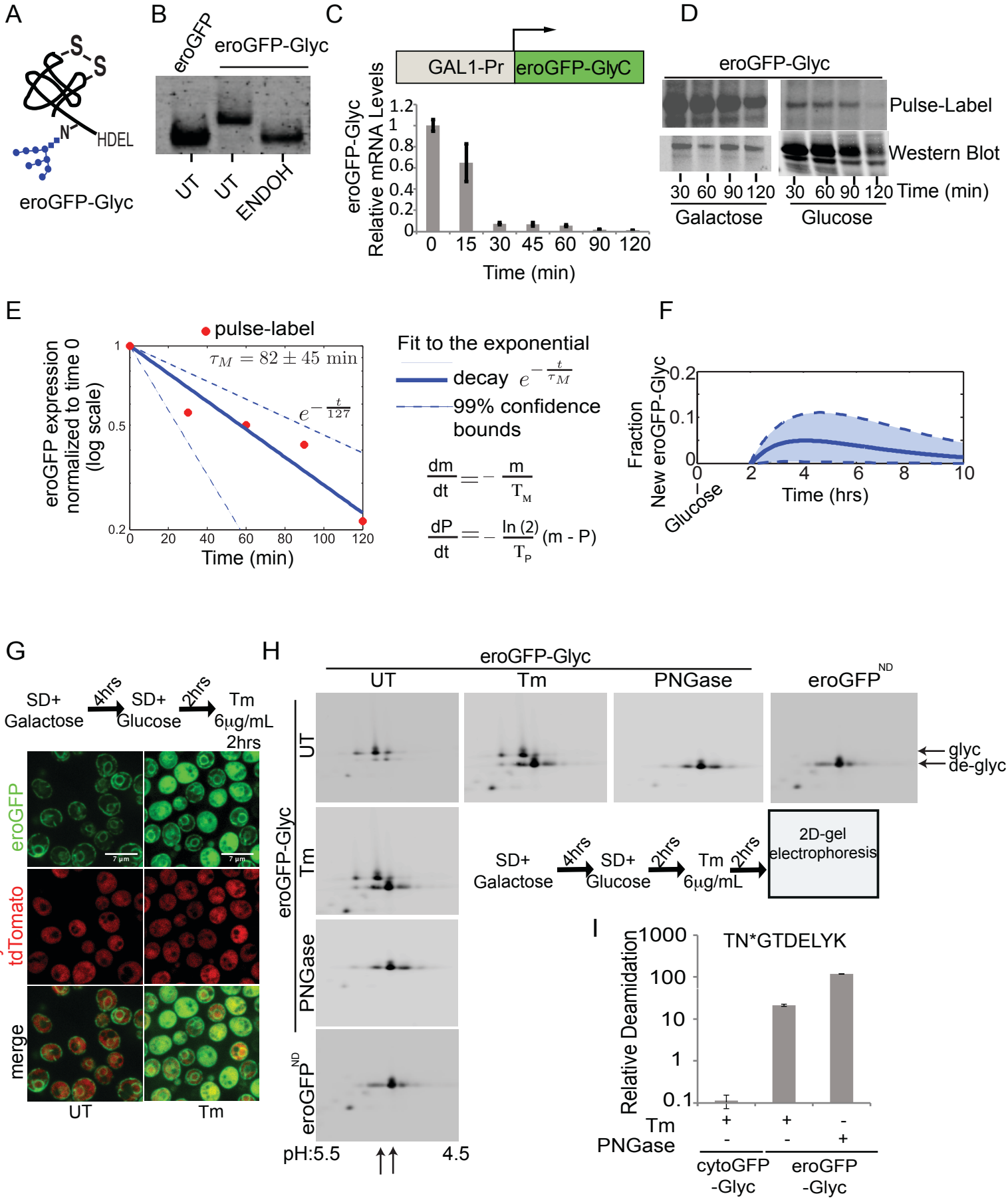

Igbaria et al Figure S2

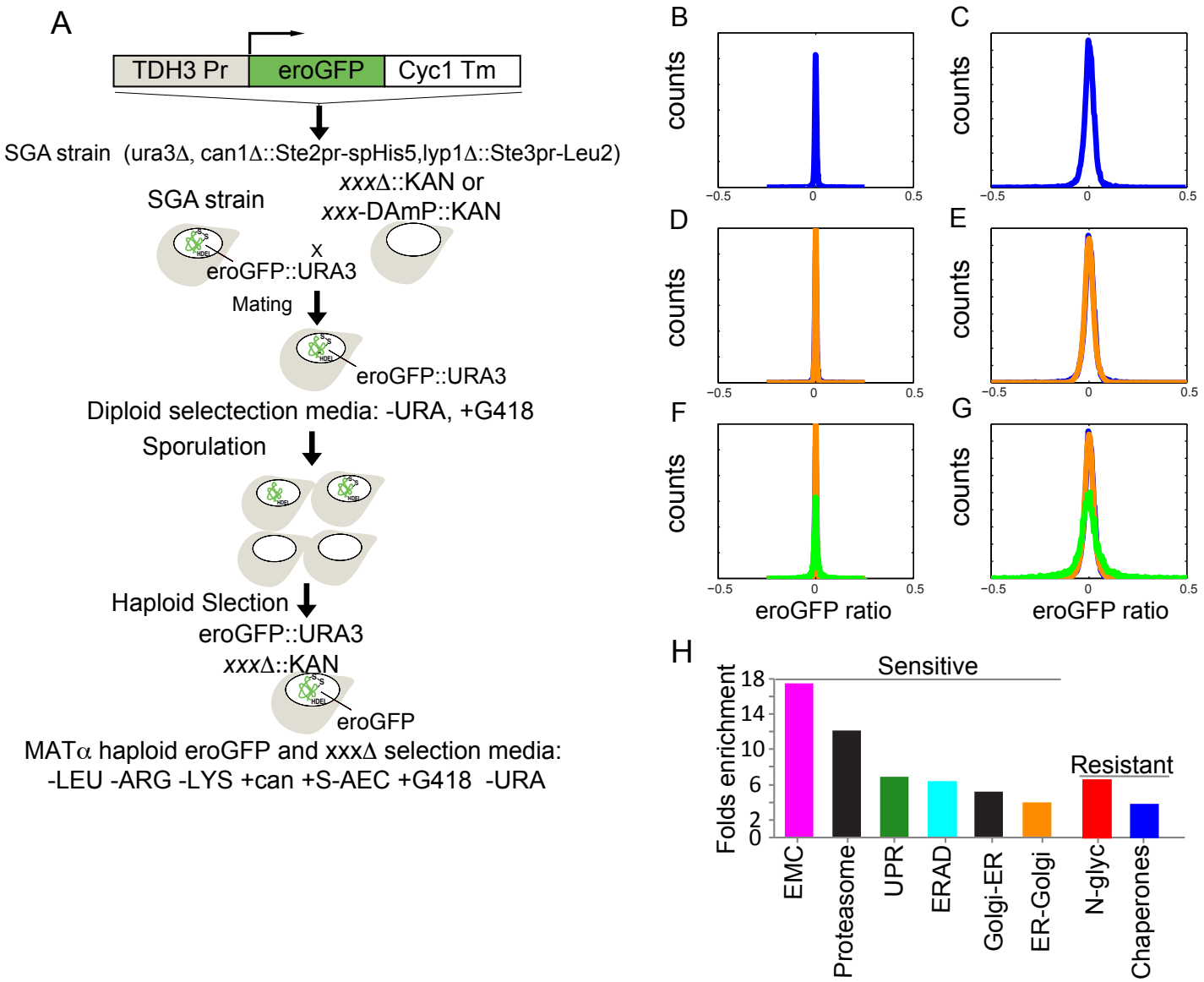

Igbaria et al Figure S3

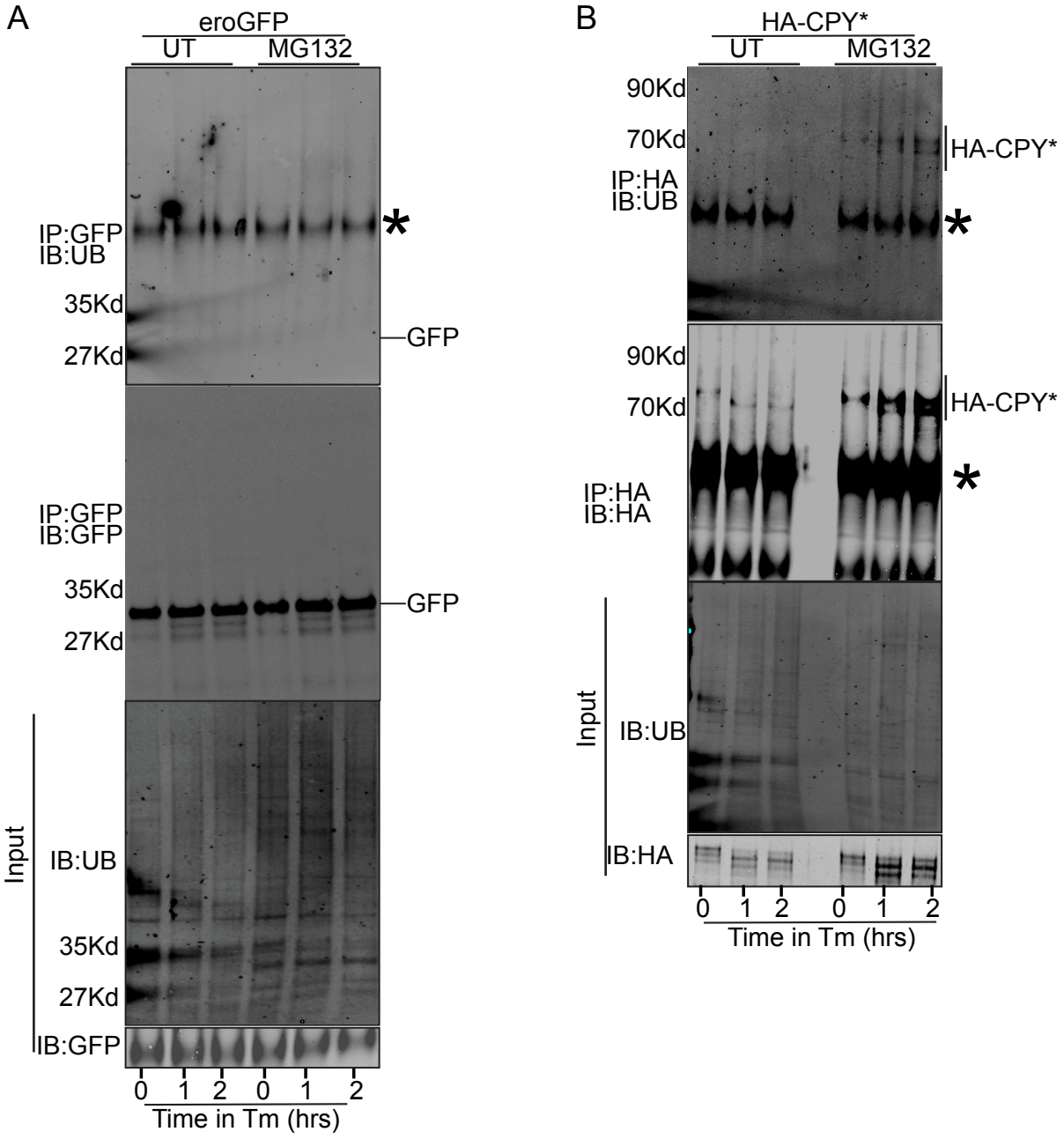

Igbaria et al Figure S4

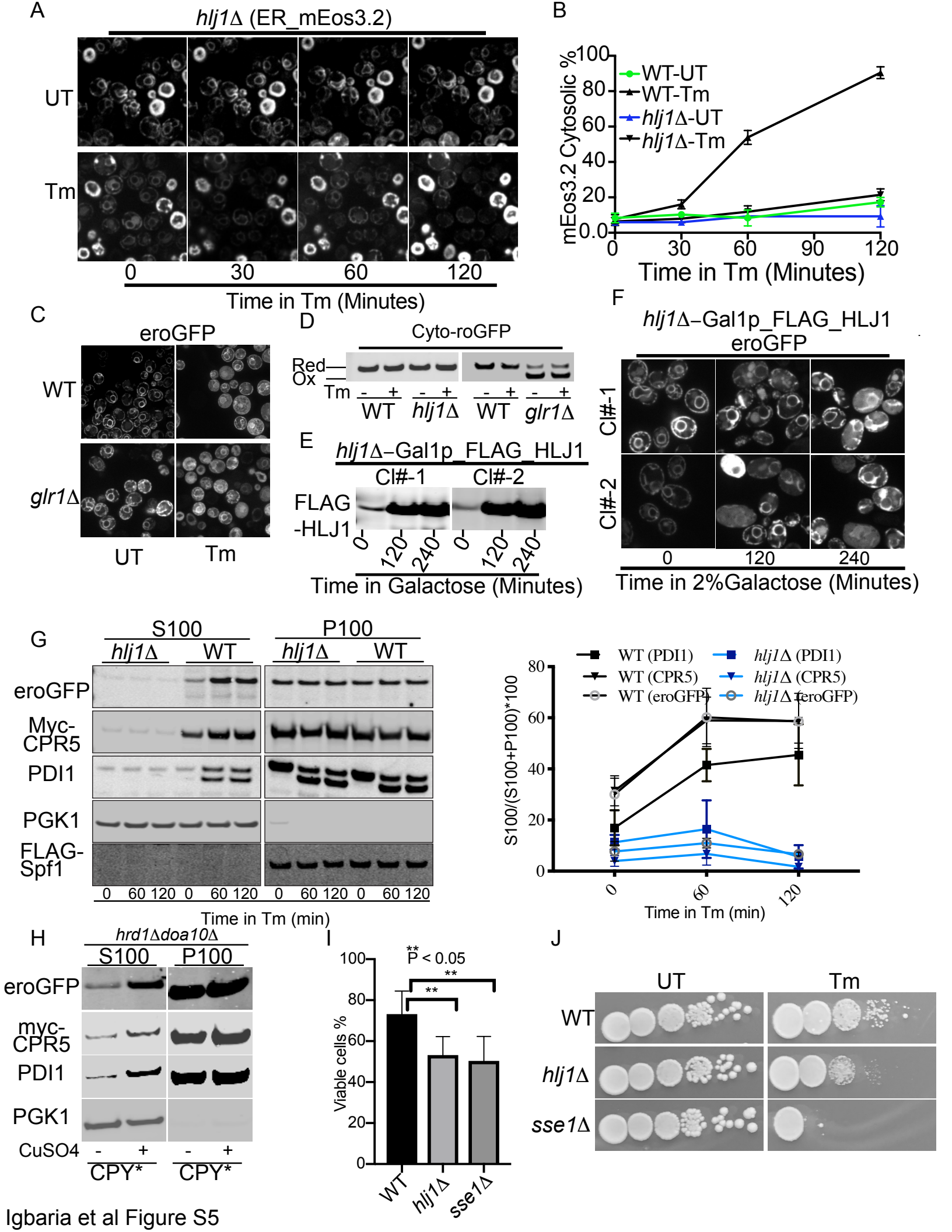

Igbaria et al Figure S5